JAM CM Journal of Applied Mathematics and Computational Mechanics 2022, 21(4), 40-51
www.amcm.pcz.pl p-ISSN 2299-9965
DOI: 10.17512/jamcm.2022.4.04 e-ISSN 2353-0588

MATHEMATICAL MODELING OF THE PHENOMENA THAT OCCUR IN A BIOLOGICAL TISSUE CONTAINING PHOTOSENSITIZER

Marek Jasiński, Maria Zadoń

Department of Computational Mechanics and Engineering
Silesian University of Technology
Gliwice, Poland
marek.jasinski@polsl.pl, maria.zadon@polsl.pl

Received: 22 April 2022; Accepted: 7 October 2022

Abstract. The aim of the study is to analyze photothermal and photochemical phenomena that occur during photodynamic therapy (PDT). In this type of therapy, under the influence of the laser, reactions take place related to the transformation of triplet oxygen form into its singlet form which is cytotoxic to the tissue. The increases in temperature resulting from the laser-tissue interaction during PDT are not big; however, they can lead to changes in tissue perfusion, which can affect oxygen delivery to the tissue. The proposed model uses optical diffusion equation, Pennes bioheat transfer equation, and reactions equations for PDT. The main findings of the analysis show the impact of temperature on the value of the perfusion coefficient and triplet oxygen distributions at the end of the treatment procedure.

MSC 2010: *65M06, 65M38, 80A20, 80A30, 80A99, 92C10*
Keywords: *bioheat transfer, optical diffusion equation, photodynamic therapy, boundary element method, finite difference method*

1. Introduction

Some medical procedures use lasers to produce desired effects in tissue. An example of such a widely used therapy is photodynamic therapy (PDT), which involves the introduction of a special substance, a so-called photosensitizer, into the body, and then photochemical reactions are induced through the action of the laser. They are mainly associated with the transition of the basic form of oxygen in the body, the triplet form, into the singlet form of oxygen. The latter form is highly cytotoxic to cancer cells, so it eventually induces their necrosis. In Type I PDT reactions, direct interaction of the excited photosensitizer is used. In Type II reactions, the photosensitizer interacts with triplet oxygen, which is then transferred to an excited singlet state [1-4].

There are many varieties of PDT, including some that use photothermal effects that occur at slightly higher temperatures in addition to photochemical effects [4]. It is important to note that even with the small temperature increases achieved in PDT, some of the parameters of the biological tissue may change.

So far, to the authors' knowledge, models related to PDT and bioheat transfer have only been considered separately; the current work attempts to fill the gap in this regard. This will allow simultaneous observation of phenomena occurring during PDT as well as during tissue heating. This constitutes a novelty of the work.

In the first step of the current analysis, the laser energy deposition in the 2D tumor tissue domain Ω was determined on the optical diffusion equation. Two types of laser impulses were considered: continuous and controlled by maintaining a set temperature on the tissue surface. Next, the results of the calculations were entered into in the PDT model consisting of coupled reaction equations for triplet oxygen, singlet oxygen, and photosensitizer, as well as in the laser heat source function in bioheat transfer equation. Additionally, in the bioheat transfer model the perfusion coefficient was assumed to be dependent on tissue damage. In the stage of numerical implementation, the first scheme of the boundary element method was used to solve the bioheat transfer problem and the finite difference method was applied to solve the optical diffusion equation and PDT model.

2. Governing equations

As already mentioned, Type II photodynamic therapy is a medical treatment that uses the interaction of light, photosensitizer, and oxygen. Complex reactions that occur during this process can be described by a set of coupled differential reaction equations. The transition of oxygen and photosensitizer from the ground state to the excited state is accompanied, among others, by the phenomena of absorption, fluorescence, energy transfer, and photobleaching, which are incorporated in these equations by appropriate coefficients. Mostly due to the complexity of the reactions during PDT, the full set of equations is simplified to a form that takes into account the concentration of the three main components, i.e., triplet oxygen, singlet oxygen, and photosensitizer [2, 3, 5]

$$\mathbf{x}\in\Omega:\quad \begin{cases} \dfrac{d[S_0]}{dt}+\gamma\sigma[S_0]\left([S_0]+\delta\right)=0, & \gamma=\dfrac{\xi\phi[{}^3\mathrm{O}_2]}{[{}^3\mathrm{O}_2]+\beta} \\ \dfrac{d[{}^3\mathrm{O}_2]}{dt}+\gamma[S_0]=\psi_{sup}, & \psi_{sup}=\psi_{sup,max}\left(1-\dfrac{[{}^3\mathrm{O}_2]}{[{}^3\mathrm{O}_2]_{init}}\right) \\ \dfrac{d[{}^1\mathrm{O}_2]_{react}}{dt}-\gamma[S_0]=0 \end{cases} \tag{1}$$

$$t=0:\quad [S_0]=[S_0]_{init},\ [{}^3\mathrm{O}_2]=[{}^3\mathrm{O}_2]_{init},\ [{}^1\mathrm{O}_2]_{react,init}=0$$

where $[S_0]$, $[^3O_2]$ and $[^1O_2]_{react}$ of unit [μM] are the sensitizer, triplet state oxygen and singlet state oxygen concentration, respectively (capital M in the unit means molar: $[M] = [\text{mol dm}^{-3}]$), parameters β [μM], σ [μM^{-1}] and ξ [$\text{cm}^2\,\text{mW}^{-1}\,\text{s}^{-1}$] are the PDT photochemical parameters defined as oxygen quenching threshold concentration, specific photobleaching ratio and specific oxygen consumption rate, respectively, δ [μM] is the low concentration correction term, ψ_{sup} [$\mu\text{M s}^{-1}$] is the oxygen supply rate and $\psi_{sup,max}$ [$\mu\text{M s}^{-1}$] is the maximum oxygen supply rate.

In (1) ϕ [W m^{-2}] denotes the total light fluence rate, which is defined as the sum of its collimated part ϕ_c and diffuse part ϕ_d. For most soft tissues the value of ϕ_d is generally dominant, so sometimes ϕ_c is neglected, especially in models related to singlet oxygen generation [2, 3, 5]. However, since in the current work combined photochemical and photothermal reactions are considered, the collimated part was taken into account, and it was defined as [4, 6]

$$\phi_c = \phi_0 \exp\left(-\frac{2y^2}{(d/2)^2}\right)\exp(-\mu_t' x) \tag{2}$$

The diffuse part is estimated by using various approximations of the radiative transport equation including the modifications of discrete ordinates method, the statistical Monte Carlo method, or the optical diffusion equation [7-10]. In the present work, the last of these approaches has been applied in the form

$$\begin{aligned} &\mathbf{x} \in \Omega: \quad D\nabla^2\phi_d - \mu_a\phi_d + \mu_s'\phi_c = 0, \quad D = \frac{1}{3(\mu_a + \mu_s')} = \frac{1}{3\mu_t'} \\ &\mathbf{x} \in \Gamma: \quad -D\,\mathbf{n}\cdot\nabla\phi_d = \frac{\phi_d}{2}, \end{aligned} \tag{3}$$

In equations (2)-(3) ϕ_0 [W m^{-2}] is the surface irradiance of the laser, d [m] is the laser beam diameter, μ_a, μ_s' and μ_t' [m^{-1}] are the absorption, effective scattering and attenuation coefficients while D is the diffusion coefficient. The impact of laser on temperature is considered through the internal source function Q_{las} [W m^{-3}]

$$Q_{las} = \mu_a \phi \tag{4}$$

which is introduced into the equation describing the bioheat transfer in the tissue domain [6, 7, 9]. In the current work, a description based on the Pennes bioheat transfer equation with adequate boundary initial conditions is used [11-15]

$$\begin{aligned} &\mathbf{x} \in \Omega: \quad c\dot{T} = \lambda\nabla^2 T + Q_V, \quad Q_V = Q_{perf} + Q_{las} + Q_{met} \\ &\mathbf{x} \in \Gamma_0: \quad q = \alpha(T - T_{amb}), \\ &\mathbf{x} \in \Gamma_c: \quad q = 0, \\ &t = 0: \quad T = T_{init}, \end{aligned} \tag{5}$$

where λ [W m^{-1} K^{-1}] is the thermal conductivity, c [J m^{-3} K^{-1}] is the volumetric specific heat, T denotes the temperature while $\dot{T}$ is its time derivative, q [W m^{-2}] is the external heat flux, Q_{perf} and Q_{met} [W m^{-3}] are the heat source functions related to perfusion and metabolism, α [W m^{-2} K^{-1}] is the convective heat transfer coefficient, T_{amb} is the surrounding temperature and T_{init} is the initial tissue temperature. The boundary Γ_0 is the external surface of the tissue, which is subjected to laser irradiation while Γ_c is the remaining part of the boundary.

The definition of the perfusion heat source function is as follows [16-18]

$$Q_{perf} = c_B w\left(T_B - T\right) \tag{6}$$

where w [s^{-1}] is the perfusion coefficient, c_B [J m^{-3} K^{-1}] is the volumetric specific heat of the blood and T_b corresponds to the arterial temperature.

In tasks involving the analysis of the effects of external impulses on the temperature field in tissue, one of the tissue damage models, such as the thermal dose, heat shock protein model or probably the most popular Arrhenius integral, is usually used. In the current work, simulations were performed for small temperature increases, which are most often not associated with permanent thermal damage to the tissue. However, based on the above-mentioned models, functions of thermophysical parameters of tissue are formulated, which allow relating real effects occurring in the tissue to the values obtained from the thermal damage model. An example of this is that the polynomial function relates the perfusion coefficient w to the Arrhenius integral of the form [6, 13, 19]

$$Arr = \int_0^{t^F} A \exp\left[-\frac{E}{RT}\right] \mathrm{d}t, \quad w = \begin{cases} \left(1 + 25Arr - 260Arr^2\right) w_0, & 0 \le Arr \le 0.1 \\ \left(1 - Arr\right) w_0, & 0.1 < Arr \le 1 \\ 0, & Arr > 1 \end{cases} \tag{7}$$

where Arr denotes the Arrhenius integral, A [s^{-1}] is the preexponential factor, E [J mol^{-1}] is the activation energy, R [J mol^{-1} K^{-1}] is the universal gas constant, w_0 is the initial perfusion coefficient. The polynomial coefficient for [0, 0.1] respond to the increase in the perfusion coefficient caused by vasodilation, while for (0.1, 1] reflect the decrease in blood flow associated with the vasculature damage.

The value $Arr = 1$ is the tissue necrosis threshold. As already mentioned in the current work, the temperature increase was kept at a fairly low level, which even with prolonged exposure to laser irradiation does not necessarily mean thermal damage of the tissue. Thus, the introduction of (7) into the model is primarily to allow observation of changes in the tissue perfusion value. It should be noted that the perfusion coefficient is often treated as an indicator of tissue thermal damage.

The Arrhenius scheme assumes that the achieved value of the damage parameter cannot decrease, in other words, irreversible tissue damage is assumed. Therefore,

the damage model has been complemented with the TTIW algorithm, which gives the possibility to reduce the damage parameter value, provided that its value does not exceed a certain threshold value defined as Arr_{rec}. After exceeding this value, the damage is estimated based on the Arrhenius integral [10].

3. Method of solution

At the stage of numerical realization the first scheme of boundary element method (BEM) and finite difference method (FDM) have been used.

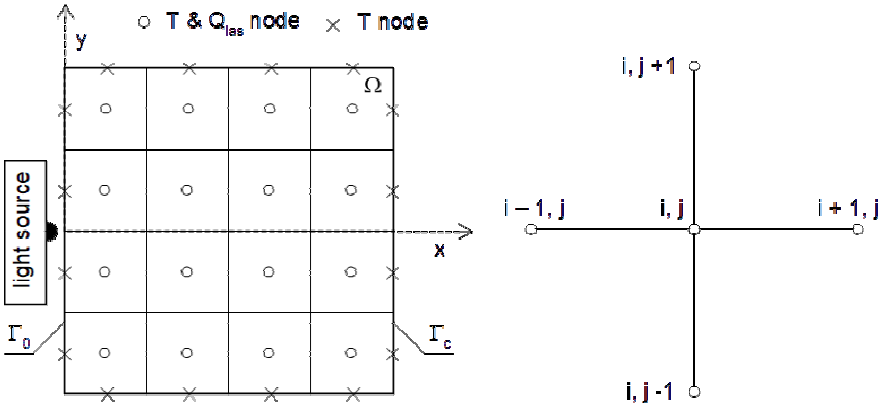

Fig. 1. The domain considered, discretization and five-point stencil

For the transient 2D bioheat diffusion problem described by (5), assuming constant time step Δt, for transition $t^{f-1} \to t^f$, the boundary integral equation takes a form [20]

$$\begin{aligned} &B(\zeta)T(\mathbf{x},t^f)+\int_\Gamma q(\mathbf{x},t^f)g(\zeta,\mathbf{x})\,\mathrm{d}\Gamma=\int_\Gamma T(\mathbf{x},t^f)h(\zeta,\mathbf{x})\,\mathrm{d}\Gamma \\ &+\iint_\Omega q^*(\zeta,\mathbf{x},t^f,t^{f-1})T(\mathbf{x},t^{f-1})\,\mathrm{d}\Omega+\iint_\Omega Q_V(\mathbf{x},t^{f-1})g(\zeta,\mathbf{x})\,\mathrm{d}\Omega \end{aligned} \tag{8}$$

where

$$h(\zeta,\mathbf{x})=\frac{1}{c}\int_{t^{f-1}}^{t^f} q^*(\zeta,\mathbf{x},t^f,t)\,\mathrm{d}t,\quad g(\zeta,\mathbf{x})=\frac{1}{c}\int_{t^{f-1}}^{t^f} T^*(\zeta,\mathbf{x},t^f,t)\,\mathrm{d}t \tag{9}$$

where T^* and q^* are the fundamental solution and the heat flux resulting from fundamental solution, $B(\zeta)$ is the coefficient from the interval (0, 1) while ζ is the observation point.

The discrete form of the equation (8) that is used in numerical realization is as follows (N – number of boundary elements, L – number of internal elements):

$$\sum_{j=1}^{N} G_{ij} q_j^f = \sum_{j=1}^{N} H_{ij} T_j^f + \sum_{l=1}^{L} P_{il} T_l^{f-1} + \sum_{l=1}^{L} Z_{il} Q_V{}_l^{f-1} \tag{10}$$

where

$$G_{ij} = \int_{\Gamma_j} g(\zeta^i, \mathbf{x}) \, \mathrm{d}\Gamma_j, \qquad H_{ij} = \begin{cases} \int_{\Gamma_j} h(\zeta^i, \mathbf{x}) \, \mathrm{d}\Gamma_j, & i \neq j \\ -0.5, & i = j \end{cases}$$
$$P_{il} = \iint_{\Omega_l} T^*(\zeta^i, \mathbf{x}, t^f, t^{f-1}) \, \mathrm{d}\Omega_l, \quad Z_{il} = \iint_{\Omega_l} g(\zeta^i, \mathbf{x}) \, \mathrm{d}\Omega_l \tag{11}$$

After determining the "missing" boundary values of the temperatures and heat fluxes, the values of the temperatures at the internal points ζ^i for time t^f are calculated using the appropriate formula ($i = N+1, ..., N+L$). Detailed information on BEM can be found in [20].

In order to solve the steady-state optical diffusion equation (3), the finite difference method was used. The following differential quotients for the five-point stencil are used (l is the grid step; cf. Fig. 1) [6, 10]

$$\left(\frac{\partial^2 \phi_d}{\partial x^2}\right)_{i,j} = \frac{\phi_{d\,i+1,j} - 2\phi_{d\,i,j} + \phi_{d\,i-1,j}}{l^2}, \quad \left(\frac{\partial^2 \phi_d}{\partial y^2}\right)_{i,j} = \frac{\phi_{d\,i,j+1} - 2\phi_{d\,i,j} + \phi_{d\,i,j-1}}{l^2} \tag{12}$$

then the form of equation (3) is as follows ($i = 1, 2, ..., N, j = 1, 2, ..., N$)

$$\phi_{d\,i,j} = \frac{D}{4D + \mu_a l^2}\left(\phi_{d\,i-1,j} + \phi_{d\,i+1,j} + \phi_{d\,i,j+1} + \phi_{d\,i,j-1}\right) + \frac{\mu_s' l^2}{4D + \mu_a l^2} \phi_{c\,i,j} \tag{13}$$

Also, for solving the PDT model (1) the finite difference method was used. In this case, the difference quotients are substituted in the place of derivative with respect to time [21-23], so the final form of difference equations takes a form

$$[S_0]_i^f = [S_0]_i^{f-1} - \Delta t \frac{\sigma \xi \phi [S_0]_i^{f-1} [{}^3\mathrm{O}_2]_i^{f-1} \left([S_0]_i^{f-1} + \delta\right)}{[{}^3\mathrm{O}_2]_i^{f-1} + \beta}$$
$$[{}^3\mathrm{O}_2]_i^f = [{}^3\mathrm{O}_2]_i^{f-1} - \Delta t \left[\frac{\xi \phi [S_0]_i^{f-1} [{}^3\mathrm{O}_2]_i^{f-1}}{[{}^3\mathrm{O}_2]_i^{f-1} + \beta} + \psi_{sup,max}\left(1 - \frac{[{}^3\mathrm{O}_2]_i^{f-1}}{[{}^3\mathrm{O}_2]_{init}}\right)\right] \tag{14}$$
$$[{}^1\mathrm{O}_2]_{react,i}^f = [{}^1\mathrm{O}_2]_{react,i}^{f-1} + \Delta t \frac{\xi \phi [S_0]_i^{f-1} [{}^3\mathrm{O}_2]_i^{f-1}}{[{}^3\mathrm{O}_2]_i^{f-1} + \beta}$$

4. Results of computations

The analysis was performed on a 4×4 cm square area of tumor tissue (Fig. 1). For BEM analysis, the interior of the domain was divided into 1600 internal constant elements, while the boundary was divided into 160 boundary elements. The following thermophysical and optical tissue parameters and values in boundary-initial conditions were assumed: $\lambda = 0.75\ \mathrm{W\,m^{-1}\,K^{-1}}$, $c = 3\text{e+}6\ \mathrm{J\,m^{-3}\,K^{-1}}$, $c_B = 3.9962\text{e+}6\ \mathrm{J\,m^{-3}\,K^{-1}}$, $w_0 = 0.00125\ \mathrm{s^{-1}}$, $Q_{met} = 250\ \mathrm{W\,m^{-3}}$, $T_B = 37°\mathrm{C}$, $\mu_a = 1.03\ \mathrm{cm^{-1}}$, $\mu'_s = 13.46\ \mathrm{cm^{-1}}$, $\alpha = 10\ \mathrm{W\,m^{-2}\,K^{-1}}$, $T_{amb} = 20°\mathrm{C}$, $T_{init} = 37°\mathrm{C}$. For the tissue damage model: $A = 1.98\text{e+}106\ \mathrm{s^{-1}}$, $E = 6.67\text{e+}5\ \mathrm{J\,mol^{-1}}$, $R = 8.314\ \mathrm{J\,mol^{-1}\,K^{-1}}$, $Arr_{rec} = 0.05$ [5, 6, 13].

The photosensitizer parameters corresponding to Photofrin at 630 nm were assumed for the PDT model: $\beta = 11.9\ \mu\mathrm{M}$, $\sigma = 7.6\text{e-}5\ \mu\mathrm{M^{-1}}$, $\xi = 3.7\text{e–}3\ \mathrm{cm^2\,mW^{-1}\,s^{-1}}$, $\delta = 33\ \mu\mathrm{M}$, and initial concentrations of $[S_0]_{init} = 7\ \mu\mathrm{M}$ and $[^3O_2]_{init} = 83$. Two values of the maximum oxygen supply rate $\psi_{sup,max} = 0.7$ and $2\ \mu\mathrm{M\,s^{-1}}$ were considered [2, 5]. The first value of the assumed maximum oxygen supply rate is therefore a more typical value for tumor tissue; the second can be regarded as a value for healthy tissue or tissue with partial presence of tumor cells. It should be noted that the values given for healthy tissue often exceed this value several times [5].

PDT treatments have different durations, most of which range from a few minutes to several minutes, but in this study a simulation time of 3600 seconds was chosen [5]. Results in the form of parameter histories are presented at two selected points in the tissue domain: $N_1(0.05, 0)$ and $N_2(0.45, 0)$ [cm], lying near the main optical axis of the laser beam.

In the first step, a series of simulations were carried out, in which dependence of the achieved temperature and thermal damage of the tissue on the laser irradiation ϕ_0, for a constant impulse and laser beam $d = 2$ mm was considered (Fig. 2). Based on these results, two values of ϕ_0 were selected for further analysis: $\phi_0 = 1500\ \mathrm{W\,m^{-2}}$ for the constant laser impulse and $\phi_0 = 2000\ \mathrm{W\,m^{-2}}$ for the impulse controlled by temperature on the external surface of the tissue Γ_0 (the impulses are marked in the figures as “const 1.5k” and “sc 2k”, respectively). In both cases the choice of ϕ_0 was guided such that the temperature reached in the tissue was equal to maximum 40°C. For the surface-controlled impulse, it was also assumed that $T_{ctrl} = 39.5°\mathrm{C}$ ±0.5°C. This means that the laser is turned off when the temperature exceeds 40°C and switched on again when the temperature drops below 39°C.

Figures 3 and 4 present the histories of temperature, Arrhenius parameter, and perfusion coefficient at two points of the tissue domain considered. As can be seen, the obtained temperatures have similar values, although, as is obvious for the surface-controlled impulse, there are oscillations around T_{ctrl}. For this type of impulse, very small values of the Arrhenius parameters were obtained, slightly affecting the value of the perfusion coefficient. For the constant impulse, the Arr_{rec} value was exceeded at point N_1, which is associated with the phase of the beginning of the vascular damage, equivalent to a decrease in perfusion below the maximum value.

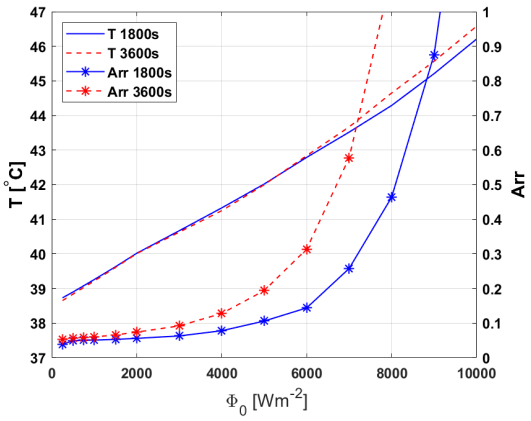

Fig. 2. Dependence of temperatures and thermal damage on laser irradiation at point N_1

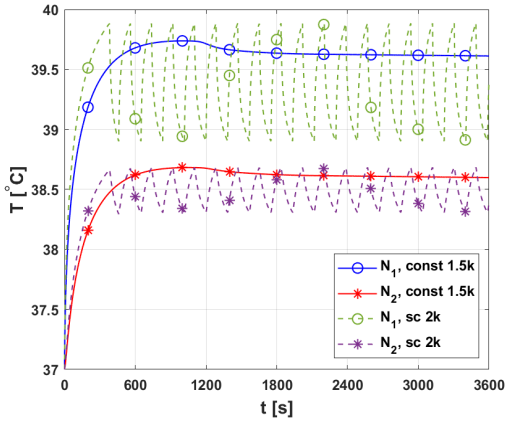

Fig. 3. History temperature at nodes N_1 and N_2

Figure 5 shows the history of $[^3O_2]$, $[S_0]$, and $[^1O_2]_{react}$ for the case $\psi_{sup,max}$ = = 0.7 μM s^{-1}. Rapid decreases can be observed for $[^3O_2]$ and $[S_0]$, and an increase for $[^1O_2]_{react}$ in the initial phase of the process. For the constant impulse and $[^3O_2]$, a return to the initial concentration is seen as the photosensitizer burns out. It can also be seen for the surface-controlled impulse that during periods when the laser is off, there is a fairly rapid increase in triplet oxygen concentration, although the initial state is not reached. It should also be noted that the results obtained are comparable to those obtained in [3] for ϕ_0 = 1500 W m^{-2}, corresponding to our impulse "const 1.5k". The results in [3] correspond to a simulation time of about 670 s, and as they relate to energy profiles on the tissue surface they were comparable with the results in point N_1.

Figures 6 and 7 compare the concentration of triplet and reacted singlet oxygen for 3600 s (the end of the simulations). It can be seen, obviously, higher $[^3O_2]$ values for $\psi_{sup,max}$ = 2 μM s^{-1}, close to the initial values and that for both cases of

surface-controlled impulses, the areas with reduced $[^3O_2]$ are smaller than for constant impulse. The final $[^1O_2]_{react}$ levels are higher for $\psi_{sup,max} = 2$ μM s^{-1}.

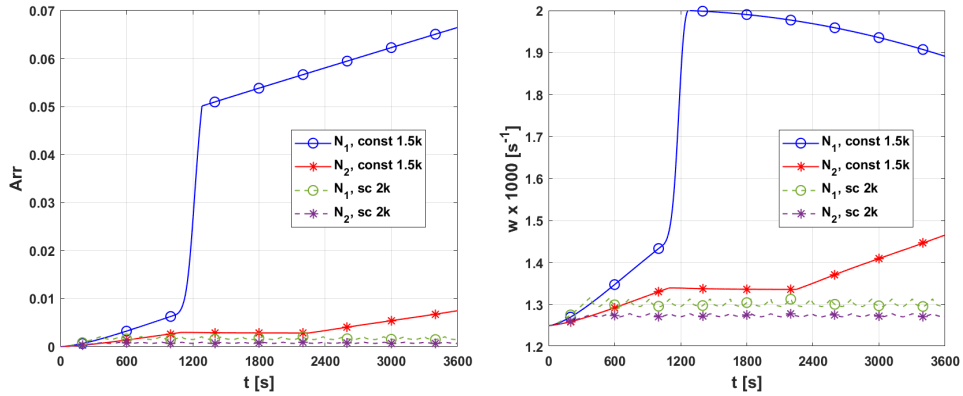

Fig. 4. History of Arrhenius parameter and perfusion coefficient at nodes N_1 and N_2

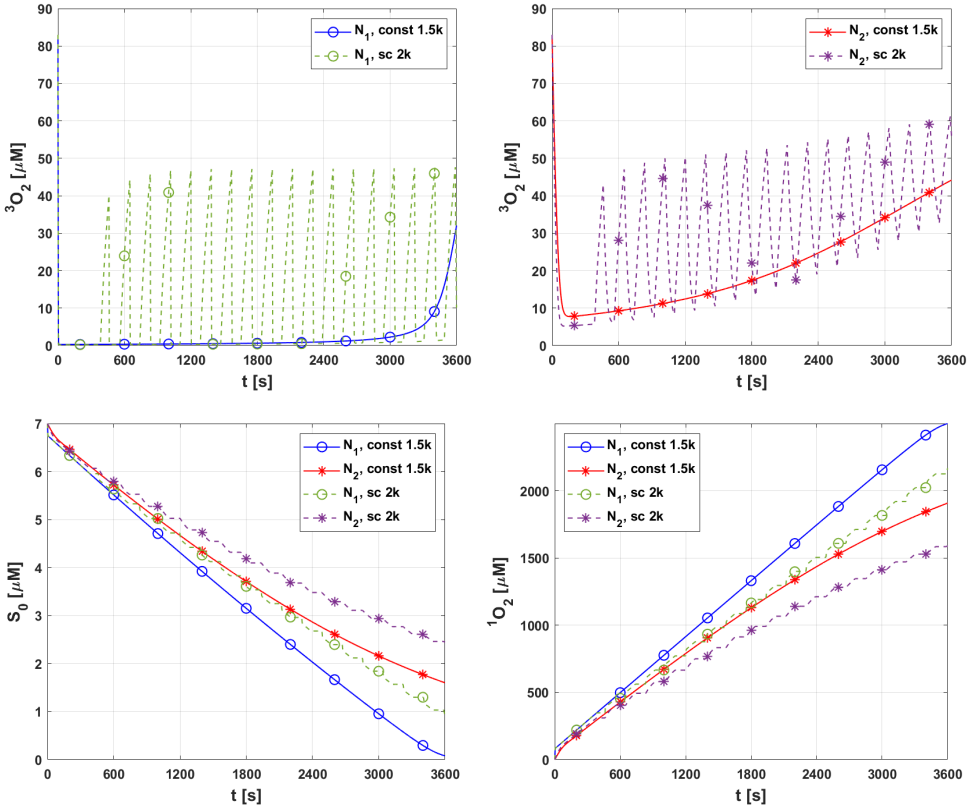

Fig. 5. History of $[^3O_2]$, $[S_0]$, and $[^1O_2]_{react}$, $\psi_{sup,max} = 0.7$ μM s^{-1}

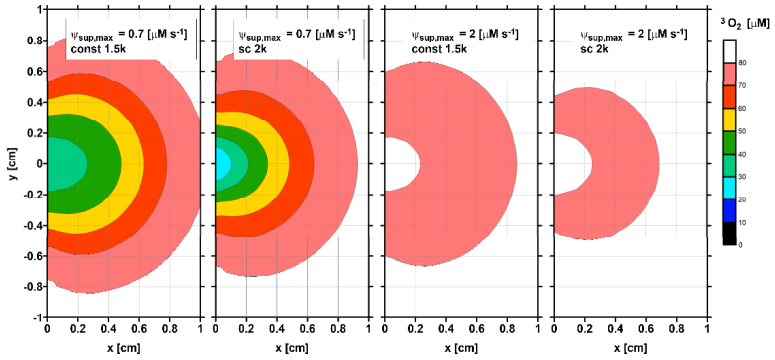

Fig. 6. Comparison of triplet oxygen concentration [$^3O_2$] for 3600 s

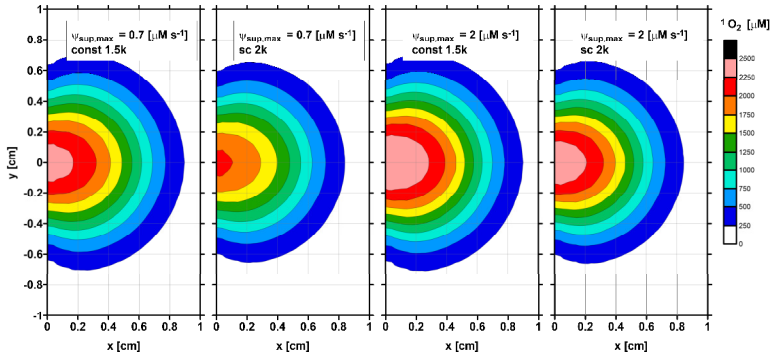

Fig. 7. Comparison of reacted singlet oxygen concentration $[^1O_2]_{react}$ for 3600 s

5. Conclusions

This paper presented the results of calculations for a model that makes it possible to simultaneously observe the reactions occurring during the PDT process as well as the accompanying thermal phenomena. So far, this type of analysis has been done separately for each chemical and thermal effects. It should be noted that although the temperature increases obtained in the simulations performed are not large and do not lead to thermal damage to the tissue, there is a noticeable change in the perfusion coefficient. Since blood is a carrier of oxygen, the presence of which is essential for the reactions occurring during PDT, it can be inferred that the change in perfusion is coupled with changes in oxygen supply to the tissues. Thus, it would be necessary to take into account the connection between bioheat transfer and PDT models that allow for such phenomena.

It was also found that, in the case of a constant impulse, there may be a small amount of thermal damage to the vascular network, which may be considered a desirable effect, occurring in addition to the main effect of PDT that produces a cytotoxic environment in the tissue. However, the use of a surface-controlled impulse can help to protect areas of tissue that are close to diseased cells. The results

of the comparisons of the final triplet and reacted singlet oxygen concentrations (Figs. 6 and 7) also show that faster photosensitizer consumption occurs in a higher value of the oxygen supply rate, which is associated with a faster return of the tissue to the initial triplet oxygen concentration, despite the higher singlet oxygen value generated.

It should be pointed out, that several issues were not considered in the current work. The tissue domain was treated as homogeneous, although many models for various cancer therapies have subdomains corresponding to healthy and tumor tissue. The fact that tumor tissue generally has a different perfusion value than healthy tissue was not taken into account. Furthermore, differences in the optical parameters of healthy and diseased tissue, and the possible change in these values as a result of photothermal phenomena, were not taken into account in a similar way as was done for the perfusion coefficient [10].

It has already been concluded that in the work of combined bioheat-PDT models, the interface to take into account the effect of temperature on oxygen transport to tissues should be taken into account. In current work the value of the oxygen supply rate $\psi_{sup,max}$ was taken in a simplified way as a constant value. This value could be derived from an appropriate model of oxygen distribution in the tissue. Such models are generally based on the concept of the Krogh cylinder and include parameters related to the presence of oxygen in the tissue and in hemoglobin, which is responsible for oxygen transport [24, 25]. Note that models of this type are considered in conjunction with thermal models, which allows, one to observe the phenomenon of hypoxia occurring as a result of thermal damage to tissue. Thus, this type of model should also become a supplement to the description of thermochemical phenomena that occur during PDT.

Acknowledgement

The research is funded from the projects Silesian University of Technology, Faculty of Mechanical Engineering.

References

[1] Abdel-Kader M.H. (ed). (2016). *Photodynamic Therapy: From Theory to Application*. Berlin, Heidelberg: Springer-Verlag.

[2] Zhu T.C., Kim M.M., Liang Xing, Finlay J.C., & Busch T.M. (2015). In-vivo singlet oxygen threshold doses for PDT. *Photononics & Lasers in Medicine*, *4*(1), 59-71.

[3] Wang, K.K., Finlay, J.C., Busch, T.M., Hahn, S.M., & Zhu, T.C. (2010). Explicit dosimetry for photodynamic therapy: macroscopic singlet oxygen modeling. *Journal of Biophotonics*, *3*(5-6), 304-318.

[4] Niemz, M.H. (2007). *Laser-tissue Interaction*. Berlin, Heidelberg, New York: Springer-Verlag.

[5] Zhu, T.C., Liu, B., & Penjweini, R. (2015). Study of tissue oxygen supply rate in a macroscopic photodynamic therapy singlet oxygen model. *Journal of Biomedical Optics*, *20*, 038001.

[6] Korczak, A., & Jasiński, M. (2019). Modelling of biological tissue damage process with application of interval arithmetic. *Journal of Theoretical and Applied Mechanics*, *57*, 249-261.

[7] Saeed, T., & Abbas, I. (2022). Finite element analyses of nonlinear DPL bioheat model in spherical tissues using experimental data. *Mechanics Based Design of Structures and Machines*, *50*, 1287-1297.

[8] Dombrovsky, L.A., Randrianalisoa, J.H., Lipinski, W., & Timchenko, V. (2013). Simplified approaches to radiative transfer simulations in laser induced hyperthermia of superficial tumors. *Computational Thermal Sciences*, *5*(6), 521-530.

[9] Alzahrani, F., & Abbas, I. (2022). A numerical solution of nonlinear DPL bioheat model in biological tissue due to laser irradiations. *Indian Journal of Physics*, *96*, 377-383.

[10] Jasiński, M. (2018). Numerical analysis of soft tissue damage process caused by laser action. *AIP Conference Proceedings*, 1922, 060002.

[11] El-Nabulsi, R.A. (2021). Fractal Pennes and Cattaneo-Vernotte bioheat equations from product-like fractal geometry and their implications on cells in the presence of tumour growth. *Journal of the Royal Society Interface*, *18*, 20210564.

[12] El-Nabulsi, R.A., & Anukool W. (2022). Nonlocal thermal effects on biological tissues and tumors. *Thermal Science and Engineering Progress*, *34*, 101424.

[13] Paruch, M. (2020). Mathematical modeling of breast tumor destruction using fast heating during radiofrequency ablation. *Materials*, *13*, 136.

[14] Paruch, M. (2017). Identification of the cancer ablation parameters during RF hyperthermia using gradient, evolutionary and hybrid algorithms. *International Journal of Numerical Methods for Heat & Fluid Flow*, *27*, 674-697.

[15] Mochnacki, B., & Ciesielski, M. (2016). Sensitivity of transient temperature field in domain of forearm insulated by protective clothing with respect to perturbations of external boundary heat flux. *Bulletin of the Polish Academy of Sciences – Technical Sciences*, *64*, 591-598.

[16] Chaundhary, R.K., Kumar, D., Rai, K.N., & Singh, J. (2021). Analysis of thermal injuries using classical Fourier and DPL models for multi-layer of skin under different boundary conditions. *International Journal of Biomathematics*, 14, 2150040.

[17] Chaundhary, R.K., Kumar, D., Rai, K.N., & Singh, J. (2022). Numerical simulation of the skin tissue subjected to hyperthermia treatment using a nonlinear DPL model. *Thermal Science and Engineering Progress*, *34*, 2022, 101394.

[18] Giordano, M.A., Gutierrez, G., & Rinaldi, C. (2010). Fundamental solutions to the bioheat equation and their application to magnetic fluid hyperthermia. *International Journal of Hyperthermia*, *26*, 475-485.

[19] Abraham, J.P., & Sparrow E.M. (2007). A thermal-ablation bioheat model including liquid-to-vapor phase change, pressure- and necrosis-dependent perfusion, and moisture-dependent properties. *International Journal of Heat and Mass Transfer*, *50*(13-14), 2537-2544.

[20] Majchrzak, E. (2013). Application of different variants of the BEM in numerical modeling of bioheat transfer processes. *MCB: Molecular & Cellular Biomechanics*, *10*(3), 201-232.

[21] Majchrzak, E., & Mochnacki, B. (2016). Dual-phase lag equation. Stability conditions of a numerical algorithm based on the explicit scheme of the finite difference method. *Journal of Applied Mathematics and Computational Mechanics*, *15*, 89-96.

[22] Majchrzak E., Turchan L., & Dziatkiewicz J. (2015). Modeling of skin tissue using the generalized dual phase-lag equation. *Archives of Mechanics*, *67*(6), 417-437.

[23] Zhu, L., Schappeler, T., Cordeo-Tumangday, C., & Rosengart, A.J. (2009). Thermal interactions between blood and tissue: development of a theoretical approach in predicting body temperature during blood cooling/rewarming. *Advanced Numerical Heat Transfer*, *3*, 197-219.

[24] Goldman, D. (2008). Theoretical models of microvascular oxygen transport to tissue. *Microcirculation*, *15*, 795-811.

[25] Jasiński, M. (2022). Numerical analysis of thermal damage and oxygen distribution in laser irradiated tissue. *Journal of Applied Mathematics and Computational Mechanics*, *2*, 51-62.